

# Numerical and experimental case study on simultaneous optimization of blank shape and variable blank holder force trajectory in deep drawing

Satoshi Kitayama<sup>1</sup> · Hiroki Koyama<sup>2</sup> · Kiichiro Kawamoto<sup>3</sup> · Takuya Noda<sup>3</sup> · Ken Yamamichi<sup>3</sup> · Takuji Miyasaka<sup>3</sup>

Received: 13 January 2016 / Revised: 6 May 2016 / Accepted: 11 May 2016 / Published online: 31 May 2016  
© Springer-Verlag Berlin Heidelberg 2016

**Abstract** This paper shows a case study for a simultaneous optimization of blank shape and variable blank holder force (VBHF) trajectory in deep drawing, which is one of the challenging issues in sheet metal forming in industry. Blank shape directly affects the material cost. To reduce the material cost, it is important to determine an optimal blank shape minimizing earing. In addition, VBHF approach is recognized as an attractive and crucial technology for successful sheet metal forming, but the practical application is rarely reported. To resolve these issues, the simultaneous optimization of blank shape and VBHF trajectory is performed. First, the experiment to identify the wrinkling region is carried out. Based on the experimental results, the finite element analysis (FEA) model is developed. The validity of the FEA model is examined by using the FLD. Numerical simulation in deep drawing is so intensive that a sequential approximate optimization (SAO) using a radial basis function (RBF) network is used for the numerical optimization. Based on the numerical result, the experiment using the AC servo press is carried out. It is found from the experimental results that the successful sheet metal forming is performed. In addition, it is confirmed from the numerical and experimental result that both the material cost and the forming energy are simultaneously reduced by using the design optimization technique.

**Keywords** Deep drawing · Variable blank holder force trajectory · Sequential approximate optimization · Radial basis function network

## 1 Introduction

Sheet metal forming is an important industrial technology for producing light weight products with high productivity. There are many process parameters for the successful sheet metal forming, such as material properties, blank shape, die geometry, and blank holder force (BHF). Low BHF leads to wrinkling, whereas high BHF results in tearing. Both wrinkling and tearing are major defects in sheet metal forming, and they should be strongly avoided. To avoid these defects, the BHF plays a crucial role in sheet metal forming. Recently, variable blank holder force (VBHF) that controls the BHF through the stroke is recognized as an attractive and innovative approach for the successful sheet metal forming (Obermeyer & Majlessi 1998), and many papers to determine the VBHF trajectory in deep drawing have been published.

Two approaches are mainly used to determine the VBHF trajectory: One is to develop a closed-loop type algorithm, and the other is to use a design optimization technique. One of the representative papers using the closed-loop type algorithm can be found in Ref. (Sheng et al. 2004), in which a proportional plus integral (PI) controller was developed. Lo and Yang (Lo & Yang 2004), Wang et al. (Wang et al. 2007), and Lin et al. (Lin et al. 2007) developed a proportional, integral, and differential (PID) controller for the VBHF trajectory in deep drawing. In their papers, wrinkling was evaluated by the distance between the die and the blank holder, and tearing was evaluated by the maximum thinning. The gain coefficients in the PI and PID controller were then adjusted to avoid the wrinkling and tearing.

✉ Satoshi Kitayama  
kitayama-s@se.kanazawa-u.ac.jp

<sup>1</sup> Kanazawa University, Kakuma-machi, Kanazawa 920-1192, Japan

<sup>2</sup> Graduate School of Natural Science and Technology, Kanazawa University, Kakuma-machi, Kanazawa 920-1192, Japan

<sup>3</sup> Komatsu Industries Corp., 1-1, Ono-machi-shinmachi, Kanazawa 920-0225, Japan

Yagami et al. developed a closed-loop type algorithm in deep drawing to avoid wrinkling (Yagami et al. 2007), in which both the BHF and the punch motion was controlled. We also developed a simple closed-loop type algorithm without the PI and PID controller (Kitayama et al. 2010), in which the thickness deviation as well as the wrinkling and tearing were considered. Through the numerical simulation and the experiments, the validity was examined. The closed-loop type algorithm is easy to carry out, but a large number of simulations are required. In particular, the trial-and-error method is required to determine the several parameters in the algorithm. In general, numerical simulation in deep drawing is so intensive that it is preferable to determine the VBHF trajectory with a small number of simulations for a practical engineering application.

To determine the VBHF trajectory with a small number of simulations, response surface approach is valid. In particular, a sequential approximate optimization (SAO) that the response surface is repeatedly constructed and optimized is recognized as one of the powerful tools available in design optimization. Chengzhi et al. determined the optimal BHF (Chengzhi et al. 2005), in which both the wrinkling and the tearing were evaluated by the forming limit diagram (FLD), and were approximated with the quadratic polynomial. Note that the BHF is constant through the punch stroke, and VBHF approach is not employed in this paper. Jakumeit et al. used the Kriging to determine the optimal VBHF trajectory (Jakumeit et al. 2005), in which the stroke was divided, and the BHF was taken as the design variables. In addition, the FLD was used to evaluate the objective functions. As Ingarao and Di Lorenzo suggest (Ingarao & Di Lorenzo 2010), the FLD is a useful tool to evaluate the wrinkling and tearing. To determine an optimal VBHF trajectory, one of the simplest approaches is to divide the stroke into sub-stroke steps. The BHF of sub-stroke step is then taken as the design variables. We also determined the optimal VBHF trajectory in deep drawing with the SAO using a radial basis function (RBF) network (Kitayama et al. 2012), in which the thickness deviation was minimized under the wrinkling and tearing constraints. Design optimization using the SAO for drawbead forces can be found in Refs. (Breitkopf et al. 2005; Jansson et al. 2003; Liu & Yang 2008; Sun et al. 2011; Wang et al. 2009a; Wang et al. 2010), in which note that a constant BHF is used. Optimization of VBHF trajectory using the SAO is recognized as an attractive and crucial approach for successful sheet metal forming in industry (Kitayama et al. 2013; Wang et al. 2008), but the practical application is rarely reported. Fortunately, servo press can freely control the BHF through the stroke, we use it for an optimal VBHF trajectory in experiment.

In addition to VBHF approach, blank shape is an important factor for successful sheet metal forming. Wrinkling will be easily generated with a large blank shape, whereas it is difficult to obtain the desirable product with a small blank shape. In deep drawing, earing that is often defined as the area above the trimmed contour is generated, and the earing is discarded. Since the blank shape directly leads to the cost reduction, it is much important to determine an optimal blank shape minimizing earing as well as the optimal VBHF trajectory. To determine an optimal blank shape, there are mainly two approaches: One is to develop a closed-loop type algorithm, and the other is to use a response surface approach. A typical approach using a closed-loop type algorithm is to adopt the geometrical shape error (GSE) (Park et al. 1999; Vafaeseefat 2011; Wang et al. 2009b) and the target shape error (TSE) (Oliveira et al. 2009), in which finite element analysis (FEA) is repeatedly carried out until the GSE and TSE value becomes very small. The approach using the GSE and the TSE are valid, but a large number of simulations are required to determine an optimal blank shape. Since it is preferable to determine an optimal blank shape with a small number of simulations, the SAO to determine an optimal blank shape is an important method in practical application in industry. Several papers to determine an optimal blank shape using the SAO can be found in Refs. (Hino et al. 2006; Kitayama et al. 2015; Liu et al. 2013; Naceur et al. 2008).

Here, we would like to summarize our motivation of this paper.

- (1) Blank shape directly affects the material cost. To reduce the material cost, it is important to determine an optimal blank shape minimizing the earing.
- (2) VBHF approach is recognized as an attractive and crucial technology for successful sheet metal forming, but the practical application is rarely reported. We use AC servo press (H1F150, Komatsu Industries, Corp.) for the VBHF approach. Unfortunately, optimal VBHF trajectory is unknown in advance. The optimal VBHF trajectory is then determined.
- (3) As described above, blank shape optimization and optimization of variable blank holder force trajectory was separately performed. Simultaneous optimization of both blank shape and VBHF trajectory is one of the crucial issues in industrial requirement, but this is rarely discussed. To meet this requirement, simultaneous optimization of both blank shape and VBHF trajectory is performed, where the SAO using the RBF network is adopted (Kitayama et al. 2011). The simultaneous optimization is one of the most challenging issues in industry. The validity should be examined through numerical and experimental result.

The rest of paper is organized as follows: In section 2, the FEA model based on the experimental results is developed. The validity of the FEA model is discussed. In section 3, the simultaneous design optimization of both blank shape and VBHF trajectory is described. The SAO using the RBF network is also briefly described. In section 4, numerical and experimental result is shown and the validity of the proposed approach is discussed.

## 2 Experiments and finite element analysis model

In our case study, a tray-type product shown in Fig. 1 is considered. First, the experiment for the formability is carried out. Based on the experimental results, the FEA model is developed. SUS304 is used as the blank, and the material property is listed in Table 1. The detailed numerical simulation model is discussed in section 2.2, and here let us explain about the forming process using the FEA model shown in Fig. 2. For the symmetry, only a half model is considered. The punch is fixed, and the die drops to the negative  $z$  direction with 580 mm/s. Note that the velocity of the die with 580 mm/s is used to shorten the computational time (Mass scaling is not used). We have already confirmed that there was no strain rate dependency during developing the FEA model. The BHF is applied to the positive  $z$  direction, and the stroke length is 58 mm for the successful sheet forming. The stress-strain curve is shown in Fig. 3, which can be obtained through an experiment. LS-DYNA, which is one of the dynamic explicit FEA codes, is used in the numerical simulation.

### 2.1 Experiment for formability

To investigate the formability, several constant BHF's are applied under lubrication condition. No tearing can be observed under the lubrication condition, and the aim is to identify the wrinkling region. Note that the tearing is observed without



Fig. 1 Tray-type product

Table 1 Material property of SUS304

Full blank size [mm] (Thickness × Length × Width)	0.38 × 430 × 250
Density: $\rho$ [kg/mm <sup>3</sup> ]	7.93 × 10 <sup>-6</sup>
Young's modulus: $E$ [MPa]	2.13 × 10 <sup>5</sup>
Poisson's ratio: $\nu$	0.26
Yield stress: $\sigma_Y$ [MPa]	294
Normal anisotropy coefficient: $r$	1
Strain hardening coefficient: $N$	0.47

lubrication. The result is shown in Fig. 4, in which the gray zone represents the wrinkling region. Let us explain about Fig. 4, in which the triangles represent the critical point that the wrinkling is observed. For example, in the case of 50 kN, no wrinkling can be observed till the stroke of 20 mm. However, the wrinkling is observed after the stroke of 20 mm.

### 2.2 Finite element analysis model

Based on the experimental results, the FEA model shown in Fig. 2 is developed. In Fig. 2, the symbol *nelm* denotes the number of finite elements. The rigid element is used to the punch, the die, and the blank holder. Note that the drawbead is modeled in the die and the blank holder for the accurate numerical simulation. The Belytschko-Tsay shell type element

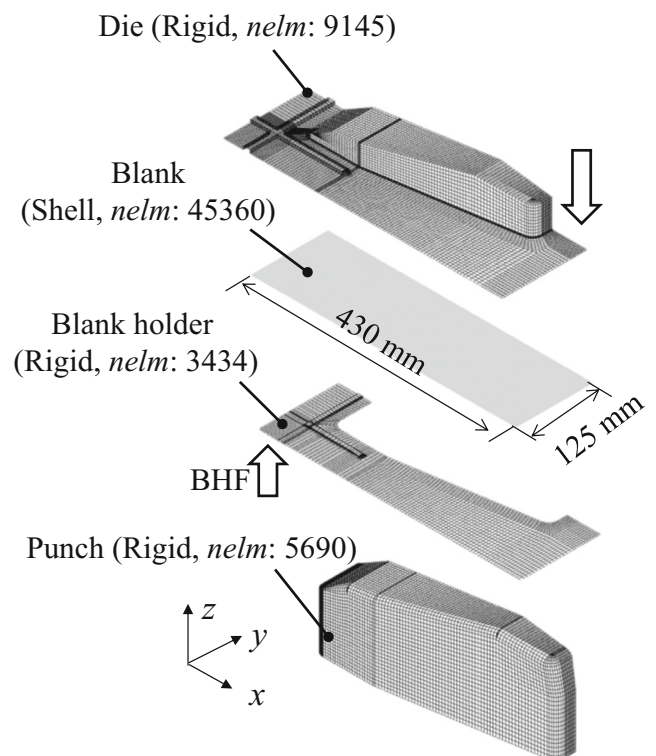


Fig. 2 Finite element analysis model for numerical simulation

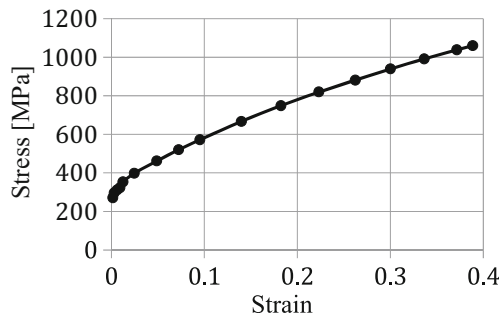


Fig. 3 Stress–strain curve

with seven integration points across the thickness is used for the blank. The friction coefficient and the penalty coefficient for contact in the interfaces (blank/punch, blank/blank holder, and blank/die) are set to 0.05 and 0.10, respectively. Note that the low friction coefficient is used for the lubrication condition. The experimental and numerical result at point A is shown in Fig. 5.

### 2.3 Forming limit diagram

In this paper, the forming limit diagram (FLD) (Storen & Rice 1975) is used to numerically evaluate the wrinkling and the tearing. In the FLD, the strain states of all elements of the blank are plotted on a major-minor strain plane. The FLD at point A in Fig. 3 is shown in Fig. 6, in which the solid curve represents the critical limit for the tearing, and the dashed line the critical limit for the wrinkling. In other words, the tearing can be observed when the strain states are plotted above the critical curve for the tearing, and the wrinkling can be observed when the strain states are plotted below the critical line for the wrinkling. It is clear from Fig. 6 that several points are plotted below the critical line for the wrinkling, and the FEA model is then valid. Then, we use this FEA model for the simultaneous optimization of blank shape and variable blank holder force trajectory.

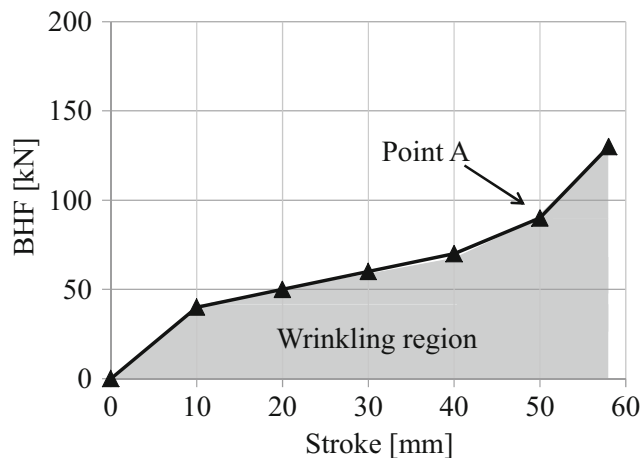


Fig. 4 Formability window of wrinkling under lubrication condition

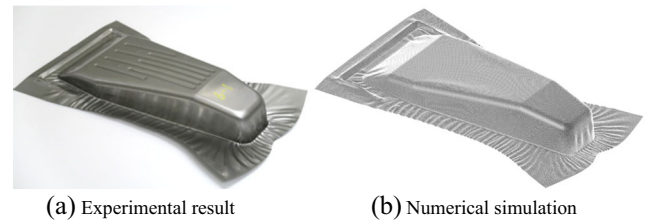


Fig. 5 Experimental and numerical result at point A in Fig. 4

## 3 Simultaneous optimization of blank shape and variable blank holder force trajectory

Simultaneous optimization of blank shape and variable blank holder force trajectory is one of the challenging issues in industry. Numerical simulation in sheet metal forming is so intensive that the SAO using the RBF network is used for the simultaneous optimization. First, we briefly the SAO using the RBF network, and the design optimization is formulated.

### 3.1 Sequential approximate optimization using radial basis function network

The general procedure of SAO is shown in Fig. 7, from which it is found that the response surface is repeatedly constructed and optimized. In addition, new sampling points are added for improving the response surface. The effectiveness using multiple surrogate techniques is discussed in Ref. (Viana et al. 2013), but the RBF network is used throughout the SAO procedure in this paper. Therefore, the RBF network is used to construct the response surface. In addition, the density function which is constructed by the RBF network is used to find an unexplored region. In the following, the RBF network is briefly described.

The RBF network is a three-layer feed-forward network. Let  $m$  be the number of sampling points, and the training data is given by  $\{x_j, y_j\} (j=1, 2, \dots, m)$ . The response surface is constructed by the following equation:

$$\hat{y}(\mathbf{x}) = \sum_{j=1}^m w_j h_j(\mathbf{x}) \tag{1}$$

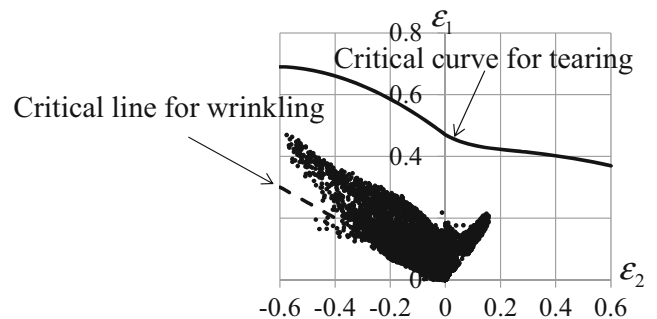


Fig. 6 Forming limit diagram at points A in Fig. 4

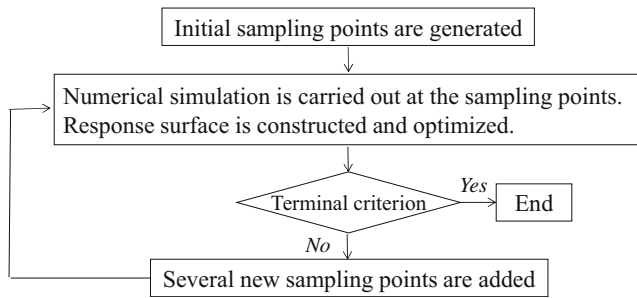


Fig. 7 General procedure of a sequential approximate optimization

where  $h_j(\mathbf{x})$  is the  $j$ -th basis function, and  $w_j$  denotes the weight of the  $j$ -th basis function. The Gaussian kernel given by (2) is widely used as the basis function:

$$h_j(\mathbf{x}) = \exp\left(-\frac{(\mathbf{x}-\mathbf{x}_j)^T(\mathbf{x}-\mathbf{x}_j)}{r_j^2}\right) \tag{2}$$

where  $r_j$  is the width of the  $j$ -th basis function. In the RBF network, in order to determine the weight vector  $\mathbf{w}$ , the following equation is minimized:

$$E = \sum_{j=1}^m (y_j - \tilde{y}(\mathbf{x}_j))^2 + \sum_{j=1}^m \lambda_j w_j^2 \rightarrow \min \tag{3}$$

where the second term is introduced for the regularization, and  $\lambda_j$  which have a sufficiently small value (e.g.  $\lambda_j = 1.0 \times 10^{-3}$ ) is introduced. The necessary condition of (3) results in the following equation:

$$\mathbf{w} = (\mathbf{H}^T \mathbf{H} + \mathbf{\Lambda})^{-1} \mathbf{H}^T \mathbf{y} \tag{4}$$

where  $\mathbf{H}$ ,  $\mathbf{\Lambda}$ , and  $\mathbf{y}$  are given as follows:

$$\mathbf{H} = \begin{bmatrix} h_1(\mathbf{x}_1) & h_2(\mathbf{x}_1) & \cdots & h_m(\mathbf{x}_1) \\ h_1(\mathbf{x}_2) & h_2(\mathbf{x}_2) & \cdots & h_m(\mathbf{x}_2) \\ \vdots & \vdots & \ddots & \vdots \\ h_1(\mathbf{x}_m) & h_2(\mathbf{x}_m) & \cdots & h_m(\mathbf{x}_m) \end{bmatrix} \tag{5}$$

$$\mathbf{\Lambda} = \begin{bmatrix} \lambda_1 & 0 & \cdots & 0 \\ 0 & \lambda_2 & \cdots & 0 \\ \vdots & \vdots & \ddots & \vdots \\ 0 & 0 & 0 & \lambda_m \end{bmatrix} \tag{6}$$

$$\mathbf{y} = (y_1, y_2, \dots, y_m)^T \tag{7}$$

It is clear from (4) that the learning of the RBF network can be achieved by the matrix inversion  $(\mathbf{H}^T \mathbf{H} + \mathbf{\Lambda})^{-1}$ . The additional learning is also reduced to the incremental calculation of the matrix inversion (Nakayama et al. 2002), and the RBF network is suitable for SAO.

In order to easily determine the width, the following simple estimate is proposed (Kitayama et al. 2011):

$$r_j = \frac{d_{j,\max}}{\sqrt{n} \sqrt{m-1}} \quad j = 1, 2, \dots, m \tag{8}$$

where  $r_j$  denotes the width of the  $j$ -th Gaussian kernel, and  $d_{j,\max}$  denotes the maximum distance between the  $j$ -th sampling point and the other sampling points. (8) is applied to each Gaussian kernel individually, and can deal with the non-uniform distribution of the sampling points.

### 3.2 Density function to find the unexplored region

One of the key issues for successful SAO is to add a new sampling point around an unexplored region for global approximation. In other words, it is important to find an unexplored region effectively. To find an unexplored region, we have developed the density function using the RBF network (Kitayama et al. 2011). The basic idea has been described in Ref. (Kitayama et al. 2011), and the numerical procedure for the density function is described below:

(D-STEP1) The vector  $\mathbf{y}^D = (1, 1, \dots, 1)_{m \times 1}^T$  is prepared at the sampling points.

(D-STEP2) The weight vector  $\mathbf{w}^D$  of the density function  $D(\mathbf{x})$  is calculated as:

$$\mathbf{w}^D = (\mathbf{H}^T \mathbf{H} + \mathbf{\Lambda})^{-1} \mathbf{H}^T \mathbf{y}^D \tag{9}$$

(D-STEP3) The density function  $D(\mathbf{x})$  is minimized to determine the unexplored region.

$$D(\mathbf{x}) = \sum_{j=1}^m w_j^D h_j(\mathbf{x}) \rightarrow \min \tag{10}$$

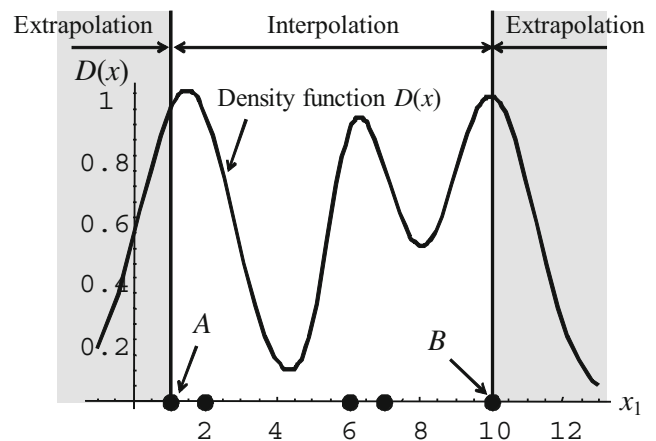


Fig. 8 Illustrative example of the density function in one dimension

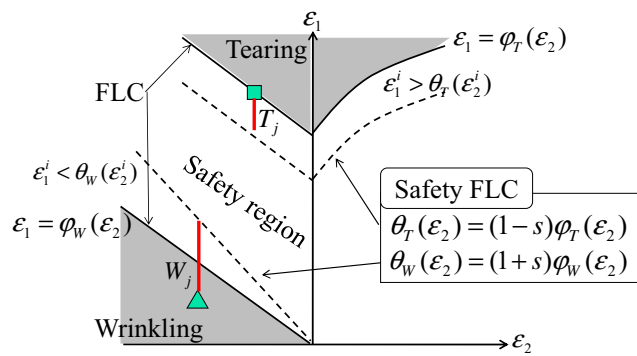


Fig. 9 Forming limit diagram for evaluating tearing and wrinkling

(D-STEP4) The point minimizing  $D(x)$  is taken as the new sampling point.

Figure 8 is an illustrative example of the density function in one dimension, and the black dots denote the sampling points. It is clear from Fig. 8 that local minima are generated around the unexplored region. Note that points A and B in Fig. 8 represent the lower and upper bounds of the design variable  $x_1$  of the density function. The optimal points minimizing the density function are taken as new sampling points for global approximation. Since it is difficult to find several optimal points simultaneously, the following iterative procedure is introduced:

- (1) A global minimum of the density function can be determined, and this point is added as a new sampling point.
- (2) The density function is constructed from all sampling points, and return to (1).

By introducing this iterative processes, it is expected that the uniform distribution of the sampling points can be achieved.

### 3.3 Evaluation of wrinkling and tearing using forming limit diagram

Tearing and wrinkling are the major defects that typically occur in deep drawing, and are handled as the design constraints in this paper. In order to evaluate the degree of tearing and wrinkling, the strains in the formed element are analyzed and compared against the forming limit curve (FLC, as shown

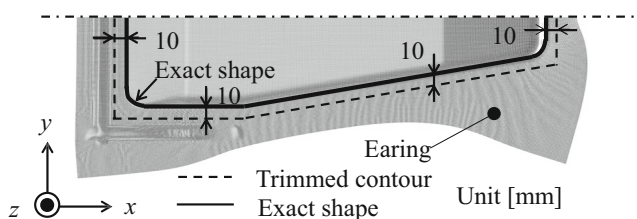


Fig. 10 Deformation in numerical simulation (only a half model)

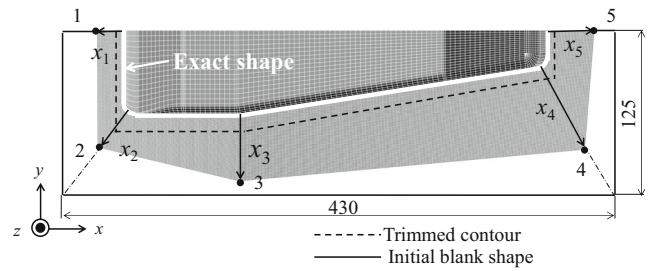


Fig. 11 Design variables for blank shape

in Fig. 9). The following FLC was defined in the principal plane of logarithmic strains proposed by Hillman and Kubli (Hillmann & Kubli 1999).

$$\varepsilon_1 = \varphi_T(\varepsilon_2) \quad \varepsilon_1 = \varphi_W(\varepsilon_2) \tag{11}$$

where  $\varphi_T$  is the FLC that controls tearing, and  $\varphi_W$  is the FLC that controls wrinkling. Then, the following safety FLC is defined:

$$\left. \begin{aligned} \theta_T(\varepsilon_2) &= (1-s)\varphi_T(\varepsilon_2) \\ \theta_W(\varepsilon_2) &= (1+s)\varphi_W(\varepsilon_2) \end{aligned} \right\} \tag{12}$$

where  $s$  represents the safety tolerance, and is defined by the engineers (in this paper,  $s$  is set to 0.2). If an element comes to or lies above FLC, it is expected that a risk of tearing can be observed. Similarly, a risk of wrinkling can be assumed if an element lies in the wrinkling region. Unlike previous studies (Wang et al. 2008; Wang et al. 2009a; Wang et al. 2010), the risk of both wrinkling and tearing were evaluated according to the following two constraints (Kitayama et al. 2012):

For tearing:

$$g_1(x) = \left( \sum_{j=1}^{nelm} T_j \right)^{1/p} \begin{cases} T_j = (\varepsilon_1^j - \theta_T(\varepsilon_2^j))^p & \varepsilon_1^j > \theta_T(\varepsilon_2^j) \\ T_j = 0 & \text{otherwise} \end{cases} \tag{13}$$

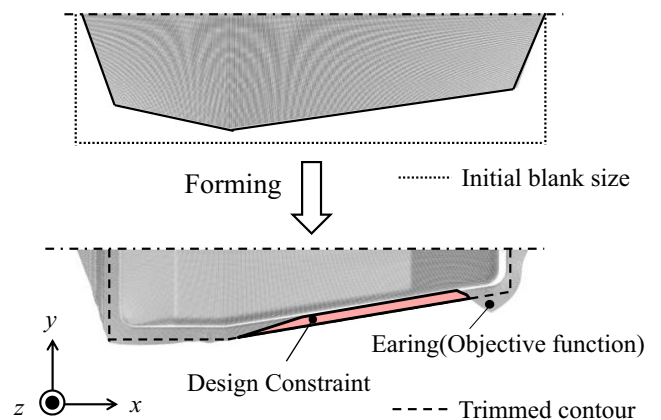


Fig. 12 Illustrative example of undesirable product

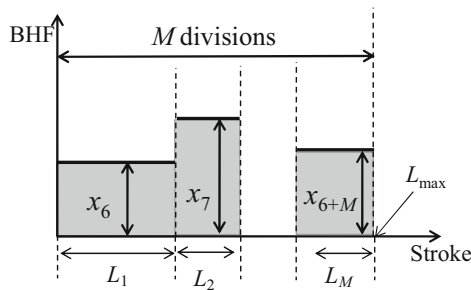


Fig. 13 Design variables for variable blank holder force trajectory

For wrinkling:

$$g_2(\mathbf{x}) = \left( \sum_{j=1}^{nelm} W_j \right)^{1/p} \begin{cases} W_j = (\theta_w(\varepsilon_2^j) - \varepsilon_1^j)^p & \varepsilon_1^j < \theta_w(\varepsilon_2^j) \\ W_j = 0 & \text{otherwise} \end{cases} \quad (14)$$

Based on the literature (Wang et al. 2008; Wang et al. 2009a; Wang et al. 2010),  $p$  is set to 4. Also,  $nelm$  represents the number of finite elements of the blank.

### 3.4 Objective function, design constraint, and design variables for blank shape and variable blank holder force trajectory

Blank shape has a direct influence on the material cost as well as the product quality. A large blank produces a large flange part that is trimmed off as waste, whereas a desirable product cannot be obtained with a small blank. In addition, the BHF affects the product quality. Therefore, simultaneous optimization of blank shape and BHF is one of the crucial issues. First, let us explain about the objective function and the design constraint for the blank shape. The deformation with the initial blank shape (the thickness of 0.38 mm, the width of 430 mm, and the length of 125 mm) is shown in Fig. 10, in which the solid line denotes the exact shape, the dashed line the trimmed contour, and the area above the trimmed contour the earing,

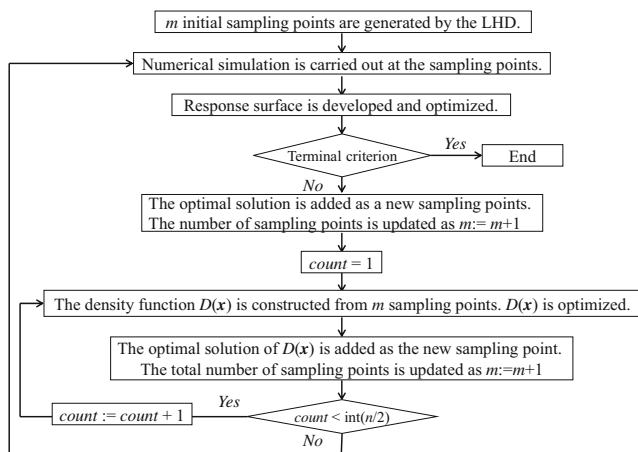


Fig. 14 Flow of sequential approximate optimization using radial basis function network

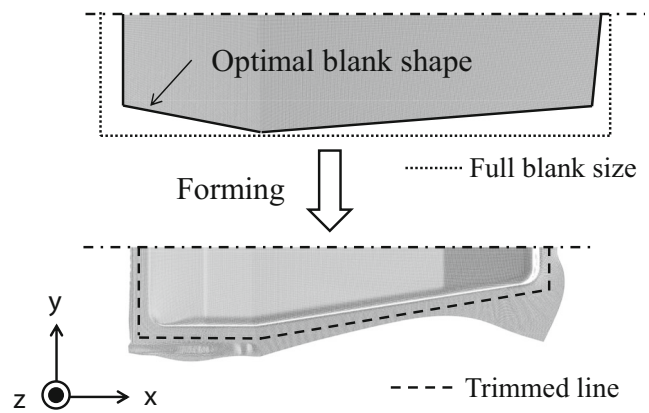


Fig. 15 Optimal blank shape and deformed shape in numerical simulation

respectively. Note that only a half model is shown in this figure. The trimmed contour is set to 10 mm from the exact shape. It is found from Fig. 10 that a large earing is produced with the initial blank size, and our objective is to determine the optimal blank shape minimizing earing. Therefore, the area above the trimmed contour is taken as the objective function.

To determine the optimal blank shape minimizing the earing, the five nodes denoted by black circles in Fig. 11 are taken as the design variables. Nodes 1 and 5 move along the horizontal line ( $x$ -axis), and Node 3 moves along the vertical line ( $y$ -axis), respectively. In addition, Nodes 2 and 4 move along the vertex of the initial blank shape. Considering the blank cutting with a laser processing, these nodes are connected by straight line as shown in Fig. 11, and the optimal blank shape is then determined.

The area above the trimmed line is taken as the objective function, and it completely depends on the blank shape. Figure 12 shows an example of the undesirable product, from which it is found that the area below the trimmed line is generated after the sheet metal forming. It is strongly needed from a design requirement that the area below the trimmed contour should not be generated. To avoid the undesirable product, the area below the trimmed contour is taken as the design

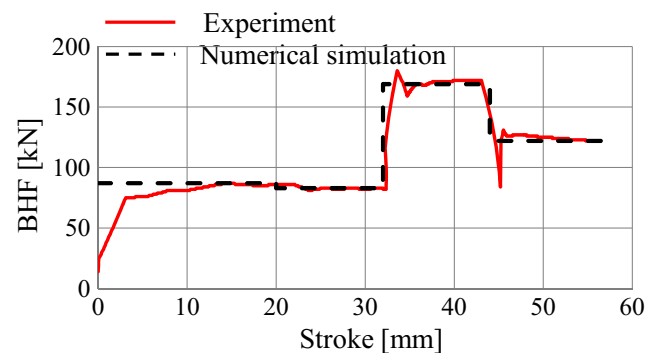


Fig. 16 Optimal VBHF trajectory in numerical simulation and experiment

**Table 2** Optimal BHF

Stroke [mm]	0–20	20–32	32–44	44–58
BHF [kN]	8.68	8.32	16.90	12.19

constraint  $g_3(x)$ . When the area below the trimmed contour is not generated as shown in Fig. 10, zero is assigned to  $g_3(x)$ .

For the variable blank holder force trajectory, total stroke  $L_{max}$  is partitioned into  $M$  sub-stroke steps and the BHF of each sub-stroke is taken as the design variables. An illustrative example of the design variables is shown in Fig. 13, where it should be noted that the design variable for VBHF starts from  $x_6$ .

### 3.5 Flow of sequential approximate optimization using radial basis function network

The flow of the SAO using the RBF network is shown in Fig. 14. The detailed procedure is summarized as follows:

- (STEP1) Several initial sampling points are generated by the latin hypercube design (LHD).
- (STEP2) Numerical simulation at the sampling points is carried out. Then, the objective function ( $f(x)$ : the area above the trimmed line), and the design constraints ( $g_1(x)$ : tearing,  $g_2(x)$ : wrinkling, and  $g_3(x)$ : the area below the trimmed contour) are calculated.
- (STEP3) Response surface by the RBF network is developed and optimized.
- (STEP4) If the terminal criterion is satisfied, the SAO using the RBF network will be terminated. Otherwise, the optimal solution obtained in STEP3 is added as a new sampling point for improving the local accuracy. In this paper, the error at the optimal solution is adopted as the terminal criterion, which is set to 5.0 %.
- (STEP5) The density function is developed and optimized for the global approximation. This step is repeated till the terminal criterion is satisfied, as shown in Fig. 13. Then, the algorithm returns to STEP 2.

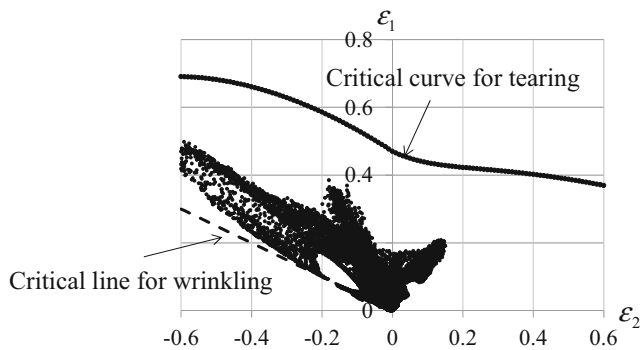


**Fig. 17** Forming limit diagram at optimal solution

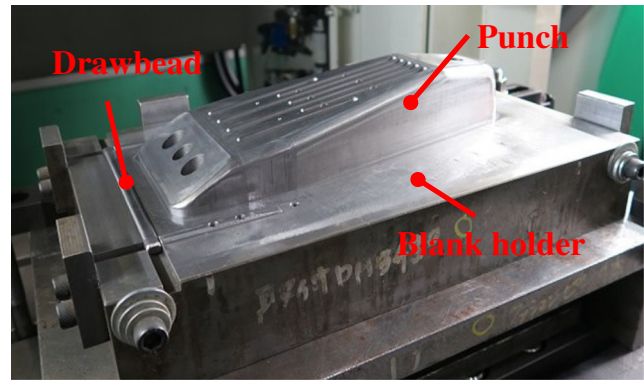


**Fig. 18** Overview of punch, blank holder, and drawbead

### 4 Numerical and experimental results

Through numerical simulation, the simultaneous optimization of blank shape and variable blank holder force trajectory is performed. Based on the numerical result, the experiment using an AC servo press (H1F150, Komatsu Industry Corp.) is carried out. Considering the availability of the AC servo press, the total stroke is divided into 4. The side constraints are set as follows:

$$\left. \begin{aligned}
 15 \leq x_1 \leq 43 [mm] & \quad 18 \leq x_2 \leq 77 [mm] & \quad 37 \leq x_3 \leq 56 [mm] \\
 40 \leq x_4 \leq 108 [mm] & \quad 34 \leq x_5 \leq 43 [mm] \\
 50 \leq x_6 \leq 130 [kN] & \quad \text{for } 0 \leq L_1 \leq 20 [mm] \\
 50 \leq x_7 \leq 200 [kN] & \quad \text{for } 20 \leq L_2 \leq 32 [mm] \\
 50 \leq x_8 \leq 200 [kN] & \quad \text{for } 32 \leq L_3 \leq 44 [mm] \\
 50 \leq x_9 \leq 200 [kN] & \quad \text{for } 44 \leq L_4 \leq 58 [mm]
 \end{aligned} \right\} \quad (15)$$

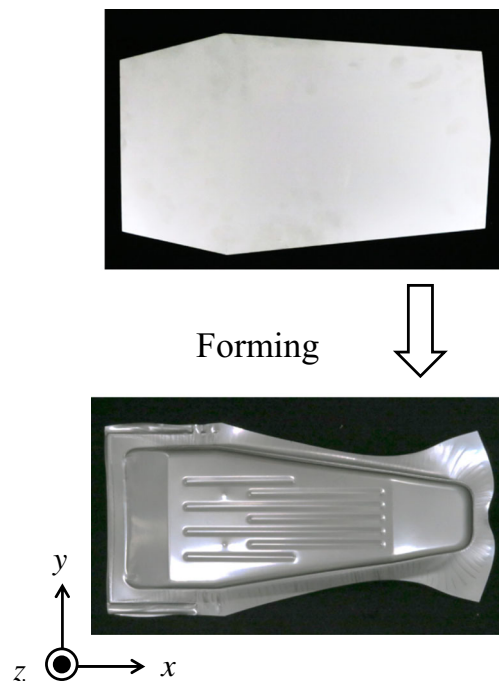


**Fig. 19** Optimal blank shape and deformed shape in experiment



**Table 3** Comparison between conventional and proposed approach

	Blank size [mm <sup>2</sup> ]	Forming energy [kJ]
Conventional approach	107,500	8.12
Proposed approach	85,890	6.47
Improvement [%]	20.10	20.30

Fifteen initial sampling points are first generated with the LHD, and the optimal blank shape and VBHF trajectory is determined. The terminal criterion is satisfied at 26 sampling points, and the SAO algorithm using the RBF network is terminated. The optimal blank shape and VBHF trajectory are shown in Figs. 15 and 16. Table 2 shows the optimal BHF. The FLD at the optimal solution is also shown in Fig. 17, from which it is found that no tearing and wrinkling can be observed.

Based on the numerical result, the experiment using AC servo press (H1F150, Komatsu Industries, Corp.) is carried out. The average die speed in the experiment is approximately 80 mm/s. The overview is shown in Fig. 18. The optimal blank shape and the deformed shape in the experiment are shown in Fig. 19. Note that the optimal VBHF trajectory is shown in Fig. 16 with the red line. It is clear from the experimental result that the successful sheet metal forming is performed. In addition, the AC servo press has a high performance for the VBHF trajectory.

Let us examine the effectiveness of optimal blank shape and optimal VBHF trajectory. Conventionally, the full blank size shown in Table 1 and a constant BHF (140kN) is used to produce this tray-type product. When the optimal blank shape is used, the area of 20.10 % can be reduced. This directly leads to the material cost reduction, and therefore the material cost of 20.10 % can be reduced with the optimal blank shape. Next, let us consider the VBHF trajectory. One of the objectives using VBHF approach is to minimize the energy consumption in the successful sheet metal forming, and the energy consumption of the AC servo

**Table 4** Dimension accuracy between numerical simulation and experiment

	<i>l</i> 1 [mm]	<i>l</i> 2 [mm]	<i>l</i> 3 [mm]	<i>l</i> 4 [mm]	<i>l</i> 5 [mm]
Numerical simulation	16.4	35.0	16.9	51.8	14.9
Experiment	16.1	32.9	14.0	51.1	14.2
Error [%]	1.9	6.4	20.7	1.4	4.9

press is evaluated. The total stroke for the successful sheet metal forming is 58 mm, and the product between the constant BHF (140kN) and the total stroke (58 mm) is then simply defined as the forming energy. The forming energy using the optimal VBHF trajectory is calculated as:

$$\sum_{i=1}^M x_{5+i} L_i \tag{16}$$

Therefore, the gray area in Fig. 13 is simply regarded as the forming energy. When the optimal VBHF trajectory is used, the forming energy of 20.30 % is reduced. The summary is listed in Table 3. Finally, as shown in Fig. 20, five lengths are examined for the dimension accuracy. The result is summarized in Table 4, from which it is clear that the error is small except for *l*<sub>3</sub>. Fortunately, as shown in Fig. 13, the area below the trimmed line is not generated with the optimal blank shape in the experiment. We confirm from these results that the simultaneous optimization of both blank shape and VBHF trajectory is valid.

### 5 Concluding remarks

Blank shape optimization and optimization of variable blank holder force trajectory was separately performed in previous papers. Simultaneous optimization of both blank shape and VBHF trajectory is recognized as one of the important issues in industrial requirement, but this is not rarely discussed. To meet this requirement, simultaneous optimization of both blank shape and VBHF trajectory is performed. First, we carried out the experiment to identify the wrinkling region. Based on the experimental results, the FEA model is developed. The validity of the FEA model is examined by using the FLD. After that, numerical optimization with the SAO using the RBF network is performed, and the optimal blank shape and the optimal VBHF trajectory are then determined. Based on the numerical optimization result, the

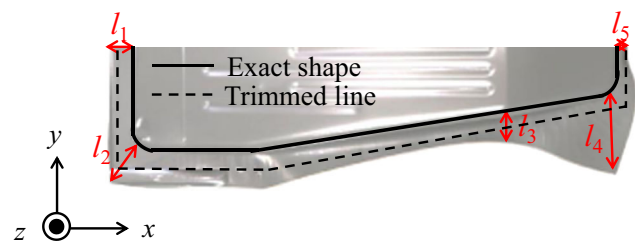


**Fig. 20** Evaluation for dimension accuracy

experiment using the AC servo press (H1F150, Komatsu Industries, Corp.) is carried out. It is found from the experimental results that the successful sheet metal forming is performed. In addition, we can confirm from the numerical and experimental result that both the material cost and the forming energy are simultaneously reduced by using design optimization technique.

**Acknowledgments** We would like to thank Horimoto Manufacturing Co. Ltd., from which the tray-type product shown in Fig. 1 is provided. The experiments using AC servo press (H1F150) were also carried out with kind cooperation of Horimoto Manufacturing Co. Ltd..

**Appendix I**

In this appendix, two optimal VBHF trajectories are determined with different objective functions. Note that the blank shape is not optimized, and the full blank size shown in Table 1 is used. The optimal VBHF trajectory is determined under tearing and wrinkling conditions. Therefore, the tearing and wrinkling are handled as the design constraints, and are evaluated as described in section 3.3. We consider the following two objective functions: (Case I) the forming energy, and (Case II) the thickness deviation. The optimal VBHF trajectory is determined through the numerical optimization. Based on the numerical result, the experiment is carried out using the AC servo press. The total stroke is divided into 4 sub-stroke steps, as shown in Fig. 21. Therefore, in both cases, the number of the design variables is 4.

**Case I**

The forming energy represented by the gray area in Fig. 21 is taken as the objective function. The optimal VBHF trajectory is shown in Fig. 22, in which the red line and the dashed line represent the optimal VBHF trajectory in the experiments and in the numerical simulation, respectively. Figure 23 shows the experimental

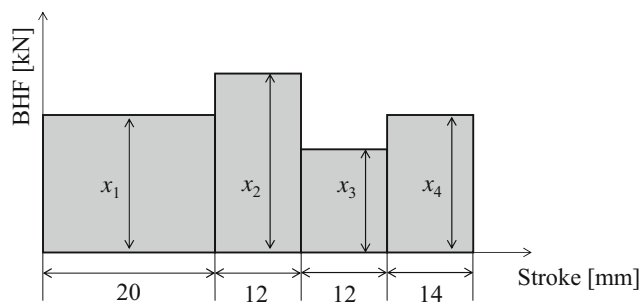


**Fig. 21** Design variables for VBHF trajectory in Cases I and II

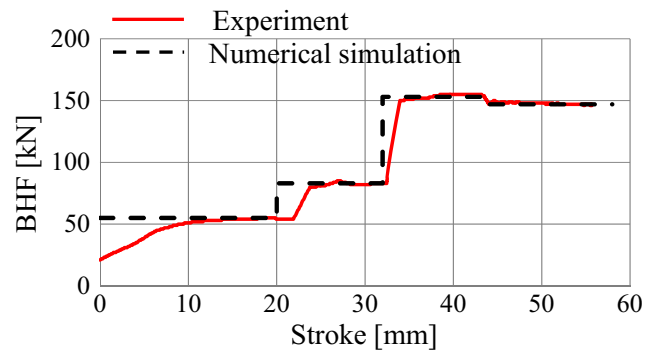


**Fig. 22** Optimal VBHF trajectory in numerical simulation and experiment of Case I

result. Figure 24 shows the lengths for dimension accuracy, and the result is summarized in Table 5.

**Case II**

Second case considers minimizing the thickness deviation, which is defined as the following equation:

$$f(\mathbf{x}) = \left\{ \sum_{i=1}^{nelm} \left( \frac{t_i}{t_0} - 1 \right)^p \right\}^{1/p} \rightarrow \min \tag{A1}$$

where  $t_i$  denotes the thickness of the  $i$ -th element of the blank,  $t_0$  the initial thickness of the blank, respectively.  $p$  in (A1) is the parameter, and is set to 4. The optimal VBHF trajectory is shown in Fig. 25, in which the red line and the dashed line represent the optimal VBHF trajectory in the experiments and in the numerical simulation, respectively. Figure 26 shows the experimental result. Figure 27 shows the lengths for dimension accuracy, and the result is summarized in Table 6.



**Fig. 23** Experimental result in Case I

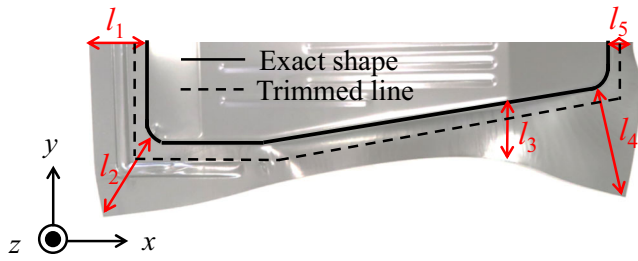


Fig. 24 Evaluation for dimension accuracy in Case I

Table 5 Dimension accuracy between numerical simulation and experiment in Case I

	$l_1$ [mm]	$l_2$ [mm]	$l_3$ [mm]	$l_4$ [mm]	$l_5$ [mm]
Numerical simulation	41.5	72.6	38.5	86.6	24.0
Experiment	42.8	70.8	38.2	84.7	24.8
Error [%]	3.0	2.5	0.8	2.2	3.2

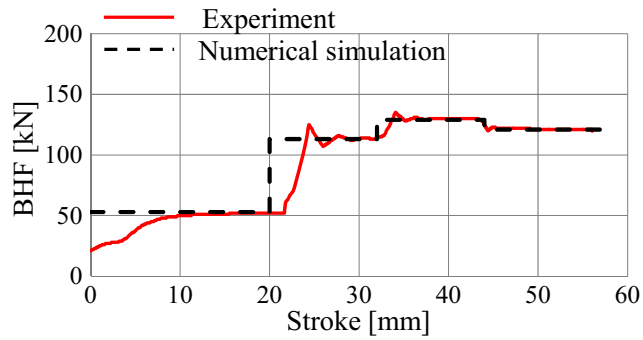


Fig. 25 Optimal VBHF trajectory in numerical simulation and experiment of Case II



Fig. 26 Experimental result in Case II

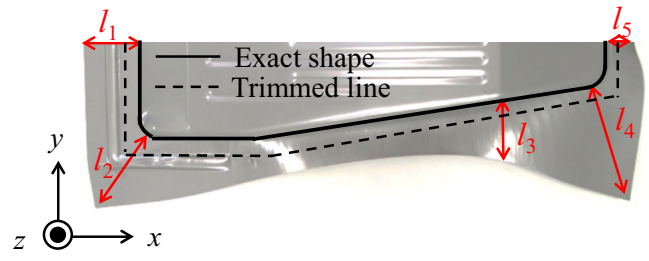


Fig. 27 Evaluation for dimension accuracy in Case II

Table 6 Dimension accuracy between numerical simulation and experiment in Case II

	$l_1$ [mm]	$l_2$ [mm]	$l_3$ [mm]	$l_4$ [mm]	$l_5$ [mm]
Numerical simulation	39.5	71.8	39.5	85.7	24.0
Experiment	41.8	70.1	38.5	85.0	24.4
Error [%]	5.5	2.4	2.6	0.8	1.6

Appendix II

Two critical lines for wrinkling and tearing of the FLD shown in Fig. 6 are drawn as follows:

The normal anisotropy coefficient  $r$  (called Lankford value) is used for the critical line for wrinkling, which is simply given by the following equation:

$$\frac{\epsilon_2}{\epsilon_1} = -\frac{1+r}{r} \tag{A2}$$

Next, the critical curve for tearing is defined as follows:

$$\epsilon_1 = \begin{cases} \frac{N}{(1+\beta) \left\{ \frac{1-N}{2} + \left[ \frac{(1+N)^2}{4} - \frac{\beta N}{(1+\beta)^2} \right]^{\frac{1}{2}} \right\}} & -1 \leq \beta \leq 0 \\ \frac{3\beta^2 + N(2+\beta)^2}{2(2+\beta)(1+\beta+\beta^2)} & 0 \leq \beta \leq 1 \end{cases} \tag{A3}$$

where  $\beta = \epsilon_2/\epsilon_1$ ,  $N$  denotes the strain hardening coefficient. A3 is solved with respect to  $\epsilon_1$ , and finally the following equations can be obtained for the critical curve for tearing:

$$\epsilon_1 = \begin{cases} \frac{1}{2}(-1-\epsilon_2 + N + \sqrt{A}) & \epsilon_2 < 0 \\ \frac{1}{6} \left[ (-3\epsilon_2 + 2N) - \frac{9\epsilon_2^2 - 4N^2}{B} + B \right] & \epsilon_2 \geq 0 \end{cases} \tag{A4}$$

where

$$\left. \begin{aligned} A &= 1 - 2\epsilon_2 - 3\epsilon_2^2 + 2N + 2\epsilon_2 N + N^2 \\ B &= \left\{ C + 9\sqrt{D} \right\}^{\frac{1}{3}} \\ C &= 81\epsilon_2^2 - 27\epsilon_2^2 N + 8N^3 \\ D &= 81\epsilon_2^4 + 9\epsilon_2^6 - 54\epsilon_2^4 N - 3\epsilon_2^4 N^2 + 16\epsilon_2^2 N^3 \end{aligned} \right\} \tag{A5}$$

For better understanding, Excel VBA code to numerically evaluate the risk of wrinkling and tearing is listed below (See Fig. 28), in which the following symbols are used:

nelm the number of finite elements of blank  
 r the normal anisotropy coefficient  $r$  (Lankford value)  
 n the strain hardening coefficient

sfact safety tolerance in (12)  
 eps1(i) major strain of the  $i$ -th element of blank, which is obtained from LS-DYNA  
 eps2(i) minor strain of the  $i$ -th element of blank, which is obtained from LS-DYNA.

**Fig. 28** Excel VBA code for numerically evaluating risk of wrinkling and tearing

```

'=====
' for wrinkling with p-norm
'=====
p = 4
sum1 = 0
For i = 1 To nelm
  thetaw(i) = -r * eps2(i) * (1 + sfact) / (1 + r)
  dis(i) = thetaw(i) - eps1(i)
  If dis(i) > 0 Then
    eval(i) = dis(i) ^ p
  Else
    eval(i) = 0
  End If
  sum1 = sum1 + eval(i)
Next i
wrinkling_risk = sum1 ^ (1 / p)
'=====
' for tearing with p-norm
'=====
sum1 = 0
For i = 1 To nelm
  If eps2(i) < 0 Then
    A = 1 - 2 * eps2(i) - 3 * eps2(i) ^ 2 + 2 * n + 2 * n * eps2(i) + n ^ 2
    thetat(i) = (1 - sfact) * (-1 - eps2(i) + n + Sqr(A)) / 2
  Else
    C = 81 * eps2(i) ^ 2 - 27 * n * eps2(i) ^ 2 + 8 * n ^ 3
    D = 81 * eps2(i) ^ 4 + 9 * eps2(i) ^ 6 - 54 * n * eps2(i) ^ 4 - 3 * (n ^ 2) * eps2(i) ^ 4 + 16 * (n ^ 3) * eps2(i) ^ 2
    B = (C + 9 * Sqr(D)) ^ (1 / 3)
    thetat(i) = (1 - sfact) * ((-3 * eps2(i) + 2 * n) - (9 * eps2(i) ^ 2 - 4 * n ^ 2) / B + B) / 6
  End If
  dis(i) = eps1(i) - thetat(i)
  If dis(i) > 0 Then
    eval(i) = dis(i) ^ p
  Else
    eval(i) = 0
  End If
  sum1 = sum1 + eval(i)
Next i
tearing_risk = sum1 ^ (1 / p)

```

## References

- Breitkopf P, Naceur H, Rassineux A, Villon P (2005) Moving least squares response surface approximation: formulation and metal forming applications. *Comput Struct* 83:1411–1428
- Chengzhi S, Guanlong C, Zhongqin L (2005) Determination the optimum variable blank-holder forces using adaptive response surface methodology (ARSM). *Int J Adv Manuf Technol* 26:23–29
- Hillmann M, Kubli W (1999) Optimization of sheet metal forming processes using simulation programs. *Numisheet '99*, Beasnc, France 1: 287–292
- Hino R, Yoshida F, Toropov VV (2006) Optimum blank design for sheet metal forming based on the interaction of high- and low-fidelity FE models. *Arch Appl Mech* 75(10):679–691
- Ingarao G, Di Lorenzo R (2010) Optimization methods for complex sheet metal stamping computer aided engineering. *Struct Multidiscip Optim* 42:459–480
- Jakumeit J, Herdy M, Nitsche M (2005) Parameter optimization of the sheet metal forming process using an iterative parallel Kriging algorithm. *Struct Multidiscip Optim* 29:498–507
- Jansson T, Nilsson L, Redhe M (2003) Using surrogate models and response surfaces in structural optimization—with application to crashworthiness design and sheet metal forming. *Struct Multidiscip Optim* 25:129–140
- Kitayama S, Hamano S, Yamazaki K, Kubo T, Nishikawa H, Kinoshita H (2010) A closed-loop type algorithm for determination of variable blank holder force trajectory and its application to square cup deep drawing. *Int J Adv Manuf Technol* 51:507–571
- Kitayama S, Arakawa M, Yamazaki K (2011) Sequential approximate optimization using radial basis function network for engineering optimization. *Optim Eng* 12(4):535–557
- Kitayama S, Kita K, Yamazaki K (2012) Optimization of variable blank holder force trajectory by sequential approximate optimization with RBF network. *J Adv Manuf Technol* 61(9–12):1067–1083
- Kitayama S, Huang S, Yamazaki K (2013) Optimization of variable blank holder force trajectory for springback reduction via sequential approximate optimization with radial basis function network. *Struct Multidiscip Optim* 47(2):289–300
- Kitayama S, Saikyo M, Kawamoto K, Yamamichi K (2015) Multi-objective optimization of blank shape for deep drawing with

- variable blank holder force via sequential approximate optimization. *Struct Multidiscip Optim* 52:1001–1012
- Lin ZQ, Wang WR, Chen GL (2007) A new strategy to optimize variable blank holder force towards improving the forming limits of aluminum sheet metal forming. *J Mater Process Technol* 183:339–346
- Liu W, Yang Y (2008) Multi-objective optimization of sheet metal forming process using Pareto-based genetic algorithm. *J Mater Process Technol* 208:499–506
- Liu Y, Chen W, Ding L, Wang X (2013) Response surface methodology based on support vector regression for polygon blank shape optimization design. *Int J Adv Manuf Technol* 66:1397–1405
- Lo SW, Yang TC (2004) Closed-loop control of the blank holding force in sheet metal forming with a new embedded-type displacement sensor. *Int J Adv Manuf Technol* 24:553–559
- Naceur H, Ben-Elechi S, Batoz JL, Knopf-Lenoir C (2008) Response surface methodology for the rapid design of aluminum sheet metal forming parameters. *Mater Des* 29:781–790
- Nakayama H, Arakawa M, Sasaki R (2002) Simulation-based optimization using computational intelligence. *Optim Eng* 3:201–214
- Obermeyer EJ, Majlessi SA (1998) A review of recent advances in the application of blank-holder force towards improving the forming limits of sheet metal parts. *J Mater Process Technol* 75:222–234
- Oliveira MC, Padmanabhan R, Baptista AJ, Alves JL, Menezes LF (2009) Sensitivity study on some parameters in blank design. *Mater Des* 30:1223–1230
- Park SH, Yoon JH, Yang DY, Kim YH (1999) Optimum blank design in sheet metal forming by the deformation path iteration method. *Int J Mech Sci* 41:1217–1232
- Sheng ZQ, Jiratheeranant S, Altan T (2004) Adaptive FEM simulation for prediction of variable blank holder force in conical cup drawing. *Int J Mach Tools Manuf* 44:487–494
- Storen S, Rice JR (1975) Localized necking in thin sheets. *J Mech Phys Solids* 23(6):421–441
- Sun G, Li G, Gong Z, He G, Li Q (2011) Radial basis function model for multi-objective sheet metal forming optimization. *Eng Optim* 43(12):1351–1366
- Vafaeseefat A (2011) Finite element simulation for blank shape optimization in sheet metal forming. *Mater Manuf Process* 26:93–98
- Viana FA, Haftka RT, Watson LT (2013) Efficient global optimization algorithm assisted by multiple surrogate techniques. *Journal of Global Optimization* 56:669–689
- Wang WR, Chen GL, Lin ZQ, Li SH (2007) Determination of optimal blank holder force trajectories for segmented binders of step rectangle box using PID closed-loop FEM simulation. *Int J Adv Manuf Technol* 32:1074–1082
- Wang H, Li GY, Zhong ZH (2008) Optimization of sheet metal forming processes by adaptive response surface based on intelligent sampling method. *J Mater Process Technol* 197:77–88
- Wang H, Li E, Li GY (2009a) The least square support vector regression coupled with parallel sampling scheme metamodeling technique and application in sheet forming optimization. *Mater Des* 30:1468–1479
- Wang J, Goel A, Yang F, Gau JT (2009b) Blank optimization for sheet metal forming using multi-step finite element simulations. *Int J Adv Manuf Technol* 40:709–720
- Wang H, Li E, Li GY (2010) Parallel boundary and best neighbor searching sampling algorithm for drawbead design optimization in sheet metal forming. *Struct Multidiscip Optim* 41:309–324
- Yagami T, Manabe K, Ymauchi Y (2007) Effect of alternating blank holder motion of drawing and wrinkle elimination on deep-drawability. *J Mater Process Technol* 187–188:187–191